Global Journal of Science Frontier Research: A
Physics and Space Science
Volume 17 Issue 3 Version 1.0 Year 2017
Type : Double Blind Peer Reviewed International Research Journal
Publisher: Global Journals Inc. (USA)
Online ISSN: 2249-4626 & Print ISSN: 0975-5896

Topological Defects: from Simplicity to Complexity

By Samo Kralj, Luka Mesarec, Pavlo Kurioz, Sylwester Rzoska & Aleš Iglič

University of Maribor

Abstract- On the one hand simple systems and simple rules can enable surprisingly complex patterns in nature. On the other hand several fundamental questions on natural behavior remain unanswered. For example, dark matter and dark energy have been introduced to explain observed structure and dynamics of the universe. However, their existence is not experimentally supported at fundamental level. It might be that difficulties in understanding of some basic phenomena of the nature arise because we are trying to present it from wrong perspective. There are strong evidences that in physics the *fields* are fundamental entities of nature and not *particles*. If this is the case then topological defects (TDs) might play the role of *fundamental particles*. An adequate testing ground to study and gain fundamental understanding of TDs are nematic liquid crystals. In this paper we present TDs in simple two-dimensional nematics emphasizing their particle-like behavior. We demonstrate strong interactions between TDs and curvature of the space which hosts them. Furthermore, we discuss how using simple rules in a simple system one can predict extremely complex behavior of lattices of TDs.

Keywords: *continuum fields, topological defects, nematic liquid crystals, topology, intrinsic curvature, extrinsic curvature.*

GJSFR-A Classification: *FOR Code: 029999*

TOPOLOGICALDEFECTSFROMSIMPLICITYTOCOMPLEXITY

Strictly as per the compliance and regulations of:

© 2017. Samo Kralj, Luka Mesarec, Pavlo Kurioz, Sylwester Rzoska & Aleš Iglič. This is a research/review paper, distributed under the terms of the Creative Commons Attribution-Noncommercial 3.0 Unported License http://creativecommons.org/licenses/by-nc/3.0/), permitting all non commercial use, distribution, and reproduction in any medium, provided the original work is properly cited.

Topological Defects: From Simplicity to Complexity

Samo Kralj [α], Luka Mesarec [σ], Pavlo Kurioz [ρ], Sylwester Rzoska [Ѡ] & Aleš Iglič [¥]

Abstract- On the one hand simple systems and simple rules can enable surprisingly complex patterns in nature. On the other hand several fundamental questions on natural behavior remain unanswered. For example, dark matter and dark energy have been introduced to explain observed structure and dynamics of the universe. However, their existence is not experimentally supported at fundamental level. It might be that difficulties in understanding of some basic phenomena of the nature arise because we are trying to present it from wrong perspective. There are strong evidences that in physics the *fields* are fundamental entities of nature and not *particles*. If this is the case then topological defects (TDs) might play the role of *fundamental particles*. An adequate testing ground to study and gain fundamental understanding of TDs are nematic liquid crystals. In this paper we present TDs in simple two-dimensional nematics emphasizing their particle-like behavior. We demonstrate strong interactions between TDs and curvature of the space which hosts them. Furthermore, we discuss how using simple rules in a simple system one can predict extremely complex behavior of lattices of TDs.

Keywords: continuum fields, topological defects, nematic liquid crystals, topology, intrinsic curvature, extrinsic curvature.

I. Introduction

Nature exhibits rich diversity of complex patterns. Several toy models [1] in nonlinear physics demonstrate that simple system and simple rules could enable complex patterns. On the other side, despite several "simplicity smoking gun" indicators, numerous fundamental questions in nature remain unanswered. Among others, we are not aware of fundamental origin of most of the energy and matter in the universe. For example, to explain observed increased acceleration of the universe *negative energy* was introduced. Furthermore, to explain observed dynamics of galaxies *dark matter* was proposed. Most probable carriers of *dark matter* are WIMPs (Weakly Interacting Massive Particles). However, despite enormous research efforts, there are no experimental evidences supporting existence of both *negative energy* and *dark matter* at fundamental level [2]. There are also unresolved discrepancies between best current theories of nature: the general relativistic theory describing phenomena at cosmological scales and quantum theory, which focuses on submicrometer scales [3]. For example, in the relativistic theory time and space coordinates are interdependent, forming the fabric of four dimensional *spacetime*. On the contrary, in quantum mechanics time is independent quantity and plays similar role as in the Newton's classical mechanics. Incompatibility of these theories is most evident in describing black holes, where both relativistic (due to their high mass) and quantum (due to their small size) effects are important.

It might be that all these unresolved problems are not satisfactorily solved yet due to wrong perspective view on nature. The best existing description of nature is given by the Standard Model of particles. It describes nature in terms of *fundamental particles* and forces among them. However, there are theorems in quantum relativistic field theory yielding contradicting claims in *particle*-view description [3]. Furthermore, several strange, counterintuitive quantum phenomena might be consequence of the fact that in hearth it is designed to explain behavior of *particles*, which from the *field*-view perspective do not exist. Several key researchers in quantum relativistic field theory shear belief that *fields* represent basic entity of nature and that nature is analogue in character [3] (i.e., it is represented by real and not integer numbers). From this perspective *fundamental particles* are emergent. They represent stable localized excitations in relevant *fields*.

Note that lord Kelvin was the first to propose *field* presentation of nature. He believed that atoms (which at that time played the role of *fundamental particles*) could be presented as stable knots in a relevant *field*. Basic principles of *field*-type description of nature were introduced by Faraday and Maxwell. Already in 1962 Skyrme [4] presented a theory in which he described hadrons as topological defects (TDs) in the *pion field*. He referred to these TDs as Skyrmions. Several latter studies proved existent of Skyrmions in diverse other condensed materials [5,6,7].

Furthermore, several predictions based on Standard Model assume that universe is essentially

Author α: Faculty of Natural Sciences and Mathematics, University of Maribor, Koroška 160, 2000 Maribor, Slovenia, Condensed Matter Physics Department, Jožef Stefan Institute, Jamova 39, 1000 Ljubljana, Slovenia. e-mail: samo.kralj@ijs.si
Author σ ¥: Laboratory of Biophysics, Faculty of Electrical Engineering, University of Ljubljana, Tržaška 25, 1000 Ljubljana.
e-mails: mesarec.luka@gmail.com (L.M.); ales.iglic@fe.uni-lj.si (A.I.)
Author ρ: Jožef Stefan International Postgraduate School, Jamova 39, 1000 Ljubljana, Slovenia. e-mail: pavel_kuryoz@hotmail.com
Author Ѡ: Institute of High Pressure Physics of Polish Academy of Sciences, ul.Sokołowska 29/37, 01-142 Warsaw, Poland.
e-mail: sylwester.rzoska@gmail.com

© 2017 Global Journals Inc. (US)

spatially homogeneous and isotropic. This is the essence of the Cosmological Principle, which originates back from Copernicus. Its key experimental support is relatively high homogeneity of the measured Cosmic Microwave Background radiation. But this configuration of the universe is based on our limited experimentally accessible view. Namely, results of recent non-linear relativistic numerical studies [8]revealed that the universe might be strongly nonhomogeneous. It might be that vast voids of the universe are negatively curved. If this is the case then, among others, increased acceleration of the universe could be explained within the existing Standard Model, with no need to introduce *dark energy*. Furthermore, its positive curvature parts might account for *dark matter*. From this perspective *dark energy* and *dark matter* are just artifacts emerging from wrong perspective of explaining natural behavior. *Negative curvature* of the universe might also support theory of multiverse. In next few decades experimental resolution is expected to become accurate enough to determine if the universe is curved or not.

In summary, deep understanding of geometry, topology and topological defects [9] (TDs) in continuous *fields* could resolve several open and unresolved fundamental issues in nature. Note that topological defects are unavoidable consequence of continuous symmetry breaking phase transitions (CSBPT). These could be according to Landau described in terms of relevant order parameter fields Q which are different from zero only in the symmetry broken phase [10]. In case of CSBPT the order parameter consist of two qualitatively different contributions [10]: the *amplitude field* and the *gauge field*. For example, in case of a para-ferromagnetic transition Q could be presented by a vector field $\vec{Q}=\lambda\vec{n}$, $|\vec{n}|=1$, where $\vec{n}$ is the *gauge* field vector. The *amplitude* λ describes a magnitude of the established ordering and has a unique value for given conditions. On the other hand the *gauge* field $\vec{n}$ defines a symmetry breaking direction. Any symmetry breaking direction can be selected because all are equivalent for CSBPT. This infinite degeneracy of *gaugefield* components enables formation of TDs in case the *gauge field* is locally frustrated. To prove universal appearance of TDs we stress that the 1st theory of coarsening dynamics of networks of TDs was developed in cosmology [11] in order to explain coarsening dynamics of the Higgs field in the early universe. The so called Kibble mechanisms claims that TDs can dynamically appear in a fast enough CSBPT because symmetry breaking choices of the corresponding *gauge field* are in general different in different parts of the system because they are informationally decoupled. Note that validity of the Kibble mechanism requires only i) CSBPT, and ii) causality (*i.e.*, information propagates with a finite speed).

Topological defects [9,12,13] describe stable localised *gauge* field structures which are topologically protected. Namely, for fixed boundary conditions TDs can not be eliminated. Topology is concerned with properties that are unaffected by continuous deformations. The key property of TDs is quantified by the discrete topological charge q, which is a conserved quantity. In general, it can have either positive or negative value. One commonly refers to TDs bearing $q>0$ as *defects*, and TDs characterized by $q<0$ as *antidefects*. Pairs of TDs bearing opposite values of q could annihilate each other into a defect-less state.

Numerous theoretical and numerical studies concerning topology and TDs have been performed in two-dimensional (2D) system[14,15,16,17]. Relatively simple XY-type models were used. Namely, they are well mathematically accessible and in some cases they are transparent enough to derive analytic solutions. In 2D the topological charge is commonly referred to as the winding number m[9,12,13]. Impact of topology on TDs is most visible via the Gaussian curvature K. According to the famous Gauss-Bonnet and Poincaré-Hopff theorems[18] the total winding number m_{tot} of TDs within a closed surface ζ possessing in-plane order is determined by the total surface integral of K:

$$m_{tot} = \frac{1}{2\pi}\iint_{\zeta} K d^2\vec{r}. \qquad (1)$$

Several works demonstrated[15,16,19]the electrostatic analogy where K and m play the role of an electric field and electric charges, respectively. Analytic derivations and numerical simulations reveal that positive (negative) Gaussian curvature is mathematically equivalent to a smeared negative (positive) topological charge [15,16]. Furthermore, it has been demonstrated that surfaces exhibiting regions with both positive and negative K could trigger unbinding of pairs {*defects, antidefect*} [15,16,19].

In general, geometry influences structure of an ordering field within a 2D manifold via two qualitatively different elastic contributions [18,20,21,22], refereed to as the *intrinsic* and *extrinsic* terms, respectively. For illustrative purpose we present key tendencies of these contributions for orientational in-plane ordering described by a vector field $\vec{n}$. *Intrinsic* terms penalize departures of $\vec{n}$ from surface geodesics[18].They are associated with variations of $\vec{n}$ as it would live only within the 2D curved surface. On the contrary, the *extrinsic* terms [20, 21, 23, 24] quantify elastic costs of out-of-surface gradients in $\vec{n}$. They are sensitive how 2D manifold is embedded in 3D Euclidian space. In case that local principal curvatures are different the *extrinsic* contributions generate an effective geometrically induced symmetry breaking field. Its strength increases with increasing difference between the curvatures.

© 2017 Global Journals Inc. (US)

In general both contributions are always present [20,21,22] and as a rule enforce contradicting tendencies. However, majority of theoretical studies employed covariant derivatives [14,15,16,17] in expressing free energy elastic terms of 2D ordered systems. Such approaches automatically rule out *extrinsic* contributions. Therefore, in such studies only impact of the *intrinsic* curvature was analyzed.

An ideal testing bed to study impact of curvature on TDs emphasizing universal features are various liquid crystal (LC) phases[25]. They represent an intermediate state between ordinary liquids and crystals. On one hand they flow like an ordinary liquid. In addition they possess long range orientational ordering and in some cases also quasi long range translational order. They are exceptionally experimentally accessible due do their unique combination of softness, optical anisotropy and transparency, and suitable scales of characteristic time and spatial relaxation responses. In addition they exhibit rich variety of phases and structures that exhibit practically all possible symmetries of TDs.

Could simple fields yield complexity of the nature (see Figure 1)? In the paper we illustrate how complexity might emerge using a simple uniaxial field in combination of symmetry breaking. We consider TDs in 2DnematicLC phase, emphasizing their particle-like behaviour and interaction with *intrinsic* and *extrinsic* curvature. The plan of the paper is as follows. We first present TDs and their key particle-like characteristics. In planar geometry we illustrate that TDs exhibit behaviour reminiscent to the Faraday cavity effect. Then we demonstrate impacts of *intrinsic* and *extrinsic* curvatures in closed nematic shells of spherical topology.

II. Theoretical Background

We consider TDs in thermotropical uniaxial nematic LC phase[25] which possesses only orientational long range order. For sake of simplicity we limit to LCs consisting of rod-like molecules exhibiting head-to-tail invariance at mesoscopic level. On lowering temperature *T*, the nematic phase (*N*) is entered at the critical temperature T_c via the first order CSBPT from the isotropic (*I*) phase as it is schematically shown in Figure 2. Isotropic phase features liquid-like behavior and short range order. Orientational ordering in the nematic phase is mesoscopically described by the nematic director field $\vec{n}$ which points along the local uniaxial ordering direction. In bulk equilibrium $\vec{n}$ is spatially homogeneously aligned along a single symmetry breaking direction.

Fast enough continuous symmetry breaking *I-N* phase transition temperature quench always generates TDs via the Kibble mechanism [11]. Due to causality in separate parts of a system different symmetry breaking directions are selected, see Figure 3. At merging areas of different boundary walls separating neighboring domains TDs are formed due to topological reasons. TDs might be formed also due to other reasons, for instance by frustrating boundary conditions [26,27] or strong enough curvature[15,16] of space hosting $\vec{n}$. In the paper we will focus to the latter case.

In the following subsections we first introduce topological charge of TDs for an arbitrary field. Afterwards we introduce our mesoscopic modelling used to treat TDs in 2D nematic films.

a) Topological defects and topological charge

Topological defects represent "tears" in respective order parameter field. Its key feature is the topological charge [9,12] which is conserved for any smooth deformations if boundary conditions are fixed. To calculate it we need first to introduce the order parameter space. It consists of all possible states of the *gauge field* equilibrium solutions. For example, in case of 3D ferromagnet described by the vector order parameter $\vec{Q}=\lambda\vec{n}$ the OPS forms a unit sphere. In 2D the OPS is a circle. The topological charge of a TD in a general unit vector field $\vec{n}=n_1\vec{e}_1+n_2\vec{e}_2+...n_d\vec{e}_d$ (i.e., $|\vec{n}|=1$) in a *d*-dimensional coordinate frame $\{\vec{e}_1,\vec{e}_2,..,\vec{e}_d\}$ is defined by an integral over a surface enclosing a defect[12].

$$q=\frac{1}{\Omega}\iint...\int Det\begin{vmatrix} n_1 & n_2 & ... & n_d \\ \frac{\partial n_1}{\partial u_1} & \frac{\partial n_2}{\partial u_1} & ... & \frac{\partial n_d}{\partial u_1} \\ ... & ... & ... & ... \\ \frac{\partial n_1}{\partial u_{d-1}} & \frac{\partial n_2}{\partial u_{d-1}} & ... & \frac{\partial n_2}{\partial u_{d-1}} \end{vmatrix} du_1 du_2 ... du_{d-1}. \quad (2)$$

The coordinates $\{u_1,u_2,...,u_{d-1}\}$ determine a *d-1* dimensional surface enclosing a defect, and Ω determines the "solid" angle in *d*-dimensional space (e.g., in 2D and 3D it equals to $\Omega=2\pi$ and $\Omega=4\pi$, respectively). The integral Eq.(2) reveals how many times all possible configurations of OPS are realized in the enclosed region. If this integral is zero, the region can not contain a single defect (it can contain several defects if the sum of their topological charges equals to zero).

Global Journal of Science Frontier Research (A) Volume XVII Issue III Version I Year 2017

© 2017 Global Journals Inc. (US)

In case of a two-dimensional space one can use parametrization $\vec{n} = n_1\vec{e}_1 + n_2\vec{e}_2 = \cos\theta\vec{e}_1 + \sin\theta\vec{e}_2$. In this case Eq.(2) yields

$$q \equiv m = \frac{1}{2\pi}\int Det\begin{vmatrix} n_1 & n_2 \\ \frac{\partial n_1}{\partial u} & \frac{\partial n_2}{\partial u}\end{vmatrix} du = \frac{1}{2\pi}\int\frac{\partial\theta}{\partial u}du = \frac{\Delta\theta}{2\pi}, \quad (3)$$

where the *du* determines a differential along a closed line enclosing a defect counter clockwise, and $\Delta\theta$ is the change of the angle θ on encircling the defect. In 2D one referees to *q* also as the winding number *m*. For a vector field a TD is characterized by an integer value of *m*, *i.e.* $m \in \{\pm1, \pm2, \pm3....\}$. In case of orientational ordering exhibiting head-to-tail invariance $\pm\vec{n}$, then half integer values of *m* are also allowed: $m \in \{\pm1/2, \pm1, \pm3/2....\}$. Some representative defect structures are schematically depicted in Figure 4.

b) Ordering fields and free energy

We henceforth restrict to 2D films exhibitingnematic liquid crystal ordering. We set that molecules displaying uniaxialnematic orientational ordering are bound to lie in the local tangent plane of a flat or curved surface as shown in Figure 5. Its local surface patch, corresponding to a point at mesoscopic scale, is characterised by the surface normal $\vec{\nu}$, and by the curvature tensor [28,29]

$$\underline{C} = C_1\vec{e}_1 \otimes \vec{e}_1 + C_2\vec{e}_2 \otimes \vec{e}_2. \quad (4)$$

Here the unit vectors $\{\vec{e}_1, \vec{e}_2\}$ point along the surface principal directions with principal curvatures $\{C_1, C_2\}$ as shown in Figure 6.

The localnematicorientational order is described by the nematic director field $\vec{n}$, $|\vec{n}| = 1$, which is schematically depicted in Figure 5. At the mesoscopic levelnematicmolecules are assumed to be rod-like, exhibiting the so-called head-to-tail invariance, where states $\pm\vec{n}$ are equivalent. Consequently, ordering is describedby the tensor order parameter[29]

$$\underline{Q} = \lambda\left(\vec{n}\otimes\vec{n} - \vec{n}_\perp \otimes \vec{n}_\perp\right), \quad (5)$$

For which $\underline{Q}(\vec{n}) = \underline{Q}(-\vec{n})$. The quantity λ determines the *amplitude field* and $\vec{n}$ plays the role of the *gauge field*, $\vec{\nu} = \vec{n}\times\vec{n}_\perp$, and $\vec{n}\cdot\vec{n}_\perp = 0$.

In terms of invariants in terms of $\underline{C}$ and $\underline{Q}$ we express the free energy density $f = f_c + f_e^{(\text{int})} + f_e^{(ext)}$, where we take into account only the most essential terms to demonstrate key qualitative features of our interest. Here f_c, $f_e^{(\text{int})}$, $f_e^{(ext)}$ stand for condensation, *intrinsic* elastic and *extrinsic* elastic term, respectively. We express them as

$$f_c = -ATr\underline{Q}^2 + B\left(Tr\underline{Q}^2\right)^2, \quad (6a)$$

$$f_e^{(int)} = k_i Tr\left(\nabla_s \underline{Q}\right)^2, \quad (6b)$$

$$f_e^{(ext)} = k_e Tr\left(\underline{Q}\underline{C}^2\right). \quad (6c)$$

Here *A* and *B* are positive material constants in nematic phase, and $\{k_i, k_e\}$ stand for {*intrinsic, extrinsic*} curvature elastic constants, $\nabla_s = (\underline{I} - \vec{\nu}\otimes\vec{\nu})\nabla$ stands for the surface gradient operator[29] and ∇ is 3D gradient operator.

Nematic tensor order parameters $\underline{Q}^{(3D)}$ in 3D and $\underline{Q}$ in 2D are related as

$$\underline{Q}^{(3D)} = \underline{Q} + \frac{\lambda^{(3D)}}{2}\left(3\vec{\nu}\otimes\vec{\nu} - \underline{I}\right). \quad (7)$$

In our 2D approach we assume that $\lambda^{(3D)}$ (the eigenvalue of $\underline{Q}^{(3D)}$ along $\vec{\nu}$) is spatially constant. Due to this assumption we consider only TDs with biaxial cores, which is sensible for common nematics [31]. If this is the case it is convenient to introduce the degree of biaxiality [30]

$$\beta^2 = 1 - \frac{6\left(Tr\underline{Q}^{(3D)3}\right)^2}{\left(Tr\underline{Q}^{(3D)2}\right)^3} \in [0,1], \quad (8)$$

where uniaxial states are signalled by $\beta^2 = 0$ and states exhibiting maximal biaxiality by $\beta^2 = 1$. Two dimensional β^2 plot well fingerprint TDs. Namely, $m = \pm 1/2$ are characterised by a closed $\beta^2 = 1$ ring [31]. In case of an isolated TD in bulk the ring is circular and its radius is estimated by the nematic correlation length ξ. In our modeling it is estimated by

$$\xi = \sqrt{\frac{k_i}{A}}. \quad (9)$$

In simulations we consider axial symmetric shapes exhibiting inversion symmetry. We describe the shapes using the parametrizion

$$\vec{r} = \rho(s)\cos(u)\vec{e}_x + \rho(s)\sin(u)\vec{e}_y) + \rho(s)\vec{e}_z \quad (10a)$$

in the Cartezian coordinates. In the case of ellipsoidal shapes we use the parametrization

$$\vec{r} = b(\sin(v)\cos(u)\vec{e}_x + \sin(v)\sin(u)\vec{e}_y) + a\cos(v)\vec{e}_z, \quad (10b)$$

where $v \in [0,\pi]$, $u \in [0,2\pi]$. Numerical details are described in [19].

Global Journal of Science Frontier Research (A) Volume XVII Issue III Version I Year 2017

© 2017 Global Journals Inc. (US)

III. Particle-Like Behaviour of TDs

In this section we consider TDs in nematicorientational order in 2D flat and curved geometries.

a) Planar geometry

We first treat flat nematic films, where $C_1=C_2=0$. We parametrize the nematic director field in the 2D Cartesian system $\{\vec{e}_1=\vec{e}_x, \vec{e}_2=\vec{e}_y\}$ as

$$\vec{n}=\vec{e}_1 cos\theta+\vec{e}_2 sin\theta. \tag{11}$$

Minimization of free energy given by Eq.(6) yields the Euler-Lagrange equilibrium equation $\Delta\theta=0$, where we neglected spatial variations in λ. Possible solutions have a linear dependence in a respective spatial coordinate. A possible solution, expressed in Cylindrical $\{\rho,\varphi\}$ and Cartesian $\{x,y\}$ coordinate variables, reads[25]

$$\theta=m\varphi+\theta_0=m\ ArcTan(y/x)+\theta_0, \tag{12}$$

where θ_0 is a constant. From the equivalence of states $\vec{n}(\varphi=0)$ and $\vec{n}(\varphi=2\pi)$ and taking in to account head-to-tail invariance $\pm\vec{n}$ it follows that $m\in\{0,\pm1/2,\pm1,\pm3/2....\}$ must be a discrete quantity. Cases $m=0$ describe homogeneous structures defined by θ_0. These solutions determine equilibrium $\vec{n}$ configurations in bulk unconstrained samples. Cases with $m\neq0$ correspond to topological defects. The corresponding *gauge* field profiles are shown in Figure 4 ((a): $m=1/2$, (b): $m=-1/2$, (c): $m=1$, (d): $m=-1$). A pair of TDs $\{m>0,-m\}$ is referred to as {*defect, antidefect*}. Namely, if we sum the pair one obtains a homogeneous *field* structure, where the *defect* and *antidefect* mutually annihilate. Note that solutions given by Eq.(9) exhibit singularity at the center of the coordinate system, which is removed if spatial variation of λ is taken into account. Namely, at the defect center the amplitude is melted (*i.e.,* $\lambda=0$), removing the singularity. The core size of a topological defects is approximated by the nematic correlation length ξ.

The elastic free energy density of the solution given by Eq.(9) in cylindrical coordinates equals $f_e\sim k_i\lambda^2|\nabla\theta|^2=\frac{k_i\lambda^2m^2}{\rho^2}$ where we assume that $\lambda(\rho<\xi)=0$, and m miminizes the condensation free energu density f_c. Integration of the free energy density from $\rho=\xi$ to $\rho=R$ (R determines the size of the system) yields the elastic free energy cost

$$\Delta F_e=m^2\Delta F_0, \tag{13}$$

where $\Delta F_0=2\pi k_i\lambda_{eq}^2\ln\left(\frac{R}{\xi}\right)$. From the results we infer two important conclusions. Firstly, the elastic free energy penalty diverges in the limit $R\rightarrow\infty$, signalling that a single defect can not exist. Furthermore, if we have several defects in a finite volume, from a relatively large distance they effectively act as a single defect bearing an effective charge. For example, in Figure 7a we plot a regular checkerboard array of 9 TDs with alternating charge as depicted in the following Table: $\begin{vmatrix}1 & -1 & 1\\ -1 & 1 & -1\\ 1 & -1 & 1\end{vmatrix}$. In the figure the distance between neighbouring TDs equals $5a_0$. In Figures 7 we gradually zoom out the structure from the center of the checkerboard. One sees that at a relatively large scale (Figures 7d) the system configuration resembles a TD bearing the effective charge $m=1$, which equals the total charge of the system. This illustration demonstrates that in an infinite system the total charge of TDs must be zero.

Furthermore, for a single isolated defect the local elastic free energy penalty outside the core scales as $\Delta F_e\propto m^2$, see Eq.(13). Consequently, it is energetically advantageous that the defects bearing relatively strong charges decompose into elementary charges $m_0=\pm1/2$. For example, in the case of a single $m=1$ defect it holds $\Delta F_e\propto m^2=1$, while if it decomposes into two $m_0=1/2$ elementary charges it follows that $\Delta F_e\propto(1/4)+(1/4)=(1/2)$.

Note that the solution Eq.(12) solves the linear differential equation. Therefore, liner combination of solutions is also a solution where in addition the conservation of the total topological charge must be taken into account

$$\theta=\sum_{i=1}^{N}\left(m_i\ ArcTan\left(\frac{y-y_i}{x-x_i}\right)+\theta_i\right). \tag{14}$$

Here N stands for the number of TDs, where thei-th defect is characterised by the defect's core center coordinates (x_i,y_i), strength m_i and constant θ_i. If we inserts the solution Eq.(14) into the free energy and integrate it over the (x,y) plane, we obtain the free energy expressed in terms of TDs coordinates and their charges. Consequently, the system is viewed as being composed of particle-like objects (TDs) because the field coordinates are integrated out.

Next, we numerically calculate nematic patterns exhibiting TDs on a flat plane using free energy in Eq.(6). First we consider a rectangular boundary of linear size $R>>\xi$, at which we fix the nematic director profile given by Eq.(11) where we set $\theta_0=0$ and $m>0$. Therefore, via boundary condition we enforce total topological charge of strength m inside the boundary, where we calculate the resulting nematic pattern by minimizing the free energy. In Figure 8we show the case where $m=2$. One sees that the imposed $m=2$ defect decomposes into four defects bearing elementary charges $m_0=1/2$. Furthermore, the TDs tend to

© 2017 Global Journals Inc. (US)

assemble close to boundaries in a manner to maximize their mutual separation. Positions of defect cores are well visible in Figure 8a where we plot the degree of biaxility β^2 [30]of the configuration. Namely, the cores of m_0=1/2 TDs are fingerprinted by a volcano-like rim where $\beta^2 = 1$ [31]. The resulting director profile in the central region on the system is nearly spatially homogeneous, see Figure 8b. This is even more pronounced in Figure 9, where we enforce via the spherically shaped boundary the total charge m=6. One sees that 12 elementary TDs are formed which assemble just below the enclosing surface. This structure is reminiscent to the Faraday effect in conductors (if one puts electric charges on a conducting body they assemble at its surface and the resulting electric field inside the body equals zero). Note that Faraday behaviour is in our simulations well visible for cases R/ξ >>1. Absence of electric field inside the conductor in our simulations corresponds to uniform director field in the region separated for a distance greater than ξ from the enclosing boundary.

b) *Intrinsic and extrinsic curvature*

Next we consider impact on curvature on TDs, where we consider both *intrinsic* and *extrinsic* curvature. First we present key features of both contributions on a simple example. We consider a two-dimensional manifold which is embedded in the 3D Cartesian coordinate system. We parametrize the nematicorientational ordering field in 2D film using Eq.(11). In the simplest nematic description only in terms of nematic director field the elastic free energy density is expressed as

$$f_e = k|\nabla_s \vec{n}|^2, \tag{15}$$

where k is a positive elastic constant. Considering the parametrization Eq.(8) and taking into account that the frame $\{\vec{e}_1, \vec{e}_2\}$ varies in space we express the elastic term as $f = f_e^{(int)} + f_e^{(ext)}$. The *intrinsic*($f_e^{(int)}$) and *extrinsic*($f_e^{(ext)}$) contribution are given by

$$f_e^{(int)} = k\left|\nabla_s \theta + \vec{A}\right|^2, \tag{16a}$$

$$f_e^{(ext)} = k\,\vec{n} \cdot \underline{C}^2 \vec{n}. \tag{16b}$$

The quantity $\vec{A} = \kappa_{g1}\vec{e}_1 + \kappa_{g2}\vec{e}_2$ is refereed to as the spin connection [18] and $\{\kappa_{g1}, \kappa_{g2}\}$ are geodesic curvatures along $\{\vec{e}_1, \vec{e}_2\}$. The spin connection can be expressed in terms of the Gaussian curvature as $K = |\nabla \times \vec{A}|$.

We first consider key features of the *intrinsic* term. In flat geometries, where K=0, it enforces a spatially homogeneous structure. In surface patches characterized by $K \neq 0$ the ordering is in general frustrated. Consequently, the *intrinsic* term is minimized for a locally non-homogenous pattern, *i.e.* $\nabla_s \theta = -\vec{A} = -\kappa_{g1}\vec{e}_1 + \kappa_{g2}\vec{e}_2$. The resulting non-homogeneity originates from the incompatibility of straight and parallel lines on surfaces with $|K| > 0$.

On the contrary the *extrinsic* term acts like an effective external field. Using Eq.(16b) and Eq.(11) it is expressed as $f_e^{(ext)} = k\,(C_1^2 cos^2\theta + C_2^2 sin^2\theta)$. Therefore, for k>0 it tends to align $\vec{n}$ along the principal direction exhibiting minimal absolute value of curvature.

It is to be stressed that most approaches used to study impact of curvature in 2D films expressed elastic terms using covariant derivatives. In these approaches the *extrinsic* contribution is automatically ruled out. In Figure 10 we present a simple case which illustrates the importance of *extrinsic* contribution. In the cylindrical geometry shown both director structures (a) and (b) are aligned along geodesics. Consequently, the *intrinsic* contribution is zero in both cases. This degeneracy is lifted if the *extrinsic* term is taken into account. Namely, it favors structure shown in Figure 10a aligned along the cylinder axis exhibiting zero curvature.

In the following we illustrate on simple cases impacts of *intrinsic* and *extrinsic* curvature on position as well as number of TDs where we calculate numerically nematic patterns via minimization of free energy contributions given in Eqs.(6). To simplify numerical treatment we consider closed films exhibiting axial and inversion symmetry.

We first focus on the *intrinsic* term described by $f_e^{(int)}$ in Eq.(6b) and set k_e=0. Its impact on assembling of TDs on surfaces exhibiting spatially nonhomogeneous Gauss curvature well reveals the Effective Topological Charge Cancellation (ETCC) mechanism[19]. In it we characterize each surface patch $\Delta\zeta$ by its average characteristic Gaussian curvature

$$\overline{K} = \frac{1}{\Delta\zeta}\iint_{\Delta\zeta} K d^2\vec{r}. \tag{17}$$

We assign the effective topological charge to the patch:

$$\Delta m_{eff} = \Delta m + \Delta m_K. \tag{18}$$

It consists of the topological chargeΔm of "real" TDs and the spread curvature topological charge, which we define by

$$\Delta m_K = -\frac{1}{2\pi}\iint_{\Delta\zeta} K d^2\vec{r}. \tag{19}$$

Therefore, if $\overline{K} > 0$ ($\overline{K} < 0$) then $\Delta m_K < 0$ ($\Delta m_K > 0$). The ETCC mechanism claims that in each surface patch there is the tendency to cancel Δm_{eff}, i.e., to be *topologicallyneutral*. This can be achieved either i) by redistribution of existing TDs or ii) via creation of additional pairs {*defect, antidefect*}.

© 2017 Global Journals Inc. (US)

This mechanism embodies the fact that TDs with positive (negative) topological charge are attracted to regions exhibiting negative (positive) Gaussian curvature. Figure 11 yields an example which illustrates the origin of this interaction. In the figure there is a sketch of a TD bearing $m=1$ placed on the top of a spherocylinder. In this case the total elastic penalty of the TD is confined to the cup of the spherocylinder and equals zero in its cylindrical part (there the orientational ordering is spatially homogeneous). If this TD would reside on an infinite plate its elastic energy would be infinite. Consequently, there is energetic advantage to drag a topological defect bearing $m=1$ in a region exhibiting $K>0$.

Next, we illustrate the predicting power of the ETCC mechanism regarding the curvature-driven assembling of TDs. As a reference we consider a sphere of radius R, where the Gaussian curvature is spatially homogeneous and equals to $K=1/R^2$. In this case the characteristic surface patch $\Delta\zeta$ refers to the whole sphere surface and the ETCC mechanism is exactly obeyed owing to the Gauss-Bonnet and Poincare-Hopf theorems embodied in Eq.(1). Namely, in this case $\Delta m_K = -2$ and $\Delta m = 2$, yielding $\Delta m_{eff} = 0$. For equal elastic constants Δm consists of four elementary charges $m=1/2$, residing at the vertices of a regular hypothetical tetrahedron in order to maximize their mutual separation, see Figure 12. Furthermore, in this geometry the *extrinsic* contribution is absent, because $C_1=C_2=1/R$.

If one morphs the sphere into an ellipsoid, at the poles localized regions appear with relatively high positive curvature, see the dashed line in the top panel ofFigure 13. The smeared negative Gaussian charge builds up at the poles and consequently, the "real" elementary charges $m=1/2$ are progressively dragged towards the poles if one increases the ellipsoid's prolateness as shown in Figure 14.

On the contrary, on deforming a sphere into an oblate shape the positive Gaussian curvature begins to build up at the equatorial region (see the full line in the top panel of Figure 13). Consequently, on increasing the oblateness the TDs progressively approach the equatorial line. In Figure 15 we show the case where the oblateness is strong enough to assemble TDs at the equator.

In examples above the "limit" ETCC structures, where all patches are *topologically neutral*, were reached via redistribution TDs bearing $m=1/2$ which already existed in spherical geometry. In the following we illustrate a simple case where a limit ETCC structure is realized by forming additional pairs {*defect, antidefect*}. For this purpose we deform a sphere into a dumb-bell shape shown in Figure 16a. In this process we form the region of negative Gaussian curvature which can be compensated only with negative topological charges. In order to predict changes in number of TDs on narrowing the neck of dumb-bell structures we consider a limit structure, which approximately consists of two spheres connected by a catenoid, which is shown in Figure 17. The smeared Gaussian charge of closed sphere equals to $\Delta m_K = -2$ and of the catenoid $\Delta m_K = 2$. The case where four m=-1/2 neutralize negative Gaussian curvature at the neck of a catenoid is shown in Figure 18. Therefore, in order to make *topologically neutral* all three dumb-bell characteristic (top and bottom spherical-like, and middle catenoid-like) patches, one needs $\Delta m = 2$ in spherical regions and $\Delta m = -2$ in the neck region. For this purpose one needs to create four pairs {*defect, antidefect*} if one starts from a spherical shape. In Figure 16b we depict evolution of the effective topological charge in spherical parts of the dumb-bell structure on increasing the ratio ρ_2/ρ_1(the distances are defined in Figure 16a) taking into account only the initial set of TDs present in spherical geometry. In Figures 19 we show configuration of defects just below (Figures 19a) and above(Figures 19b) the critical condition where two pairs {*defect, antidefect*} are created.

Next we consider impact of extrinsic curvature, which is in our modelling presented by $f_e^{(ext)}$ in Eq.(6c). In our simulations we set $k_i=k_e$. Note that extrinsic term plays the role only for cases where $C_1 \neq C_2$. The extrinsic term acts as an external field whose strength is proportional with $k_e|C_1-C_2|$. The curvature deviator $D=|C_1-C_2|/2$ is the invariant of the curvature tensor and can be expressed by the mean curvature $H=(C_1+C_2)/2$ and Gaussian curvature $K=C_1C_2$ as $D^2=H^2-K$ [23,24]. For $k_e>0$ it tends to align nematicorientational ordering along principal directions exhibiting minimal curvature. In Figure 20 and Figure 21 we plot TDs on prolate and oblate ellipsoid. In both geometries the curvature deviator $|C_1-C_2|/2$ (see also [23,24]) exhibits maximum in the equatorial region, see the bottom panel of Figure 13. TDs tend to be expelled from regions where the effective *extrinsic* field is strong enough. Consequently, inprolate structure TDs are dragged towards the poles (Figure 20). In this case both *intrinsic* and *extrinsic* term cooperatively push TDs towards the poles. By contrast, in oblate structure the *intrinsic* and *extrinsic* term have competing tendencies. The *intrinsic* elasticity favors to assemble TDs in the equatorial region. On the other hand the *extrinsic* term expels them from this region. In Figures 21 we show the case where the effective *extrinsic* term is strong enough to expel TDs from the equatorial region, where they would be for $k_e=0$, see Figure 15.

IV. Conclusions

In the paper we describe fundamental behavior of topological defects in two-dimensional nematic liquid crystals. TDs are stabilized by topology and

© 2017 Global Journals Inc. (US)

consequently their behavior does not depend on microscopic details. For this reason they display several universal features. Two-dimensional nematic LCs represent adequate systems to study the physical properties of TDs for the following main reasons. First of all, there exist several "natural" systems exhibiting effectively two-dimensional nematic-like orientational ordering, e.g., in anisotropic biological membranes [23,24]. In addition, such systems could be prepared experimentally by coating colloids with thin LC films, referred to as nematic shells [32,33,34]. In these systems diverse TDs could be formed and relatively easily observed using optical microscopy. Next, for such systems mathematics is relatively well developed and transparent. Combined experimental and theoretical accessibility of these systems allows one to perform controlled experiments well supported by theoretical modelling [29,35,36]. Finally, such systems are of interest for various ambitious applications in photonics and sensor applications. Of particular recent interest are LC-based sensor aimed to detect biological nano-objects [37] (lipids, proteins, viruses, bacteria…). There might be also several applications in biomedicine. For instance, very recent studies reveal that TDs in epithelium cells trigger the death and removal of cells [38]. LC shells might also pave path to design colloidal crystals [39], representing analogues of "conventional" crystals. In this analogy LC shells and TDs would play the role of atoms and their valence, respectively. Note that "colloidal chemistry" might yield even richer variety of resulting crystal structures than those observed in nature because of our ability to form diverse LC shells (i.e. "atoms") with almost arbitrary configuration of TDs.

In the paper we first consider flat nematic films. On a simple example we demonstrate how particle-like description of TDs emerges, although TDs represent only relatively energetically costly singularities in nematic director field. We illustrate that TDs of relatively strong topological charge are difficult to form because they have strong tendency to decompose into *elementary* topological charges. In case of nematics these carry topological charge (winding number) $m_0=\pm 1/2$. We demonstrate the Faraday effect-like behavior in cases where we enforce a relatively strong total topological charge m within an area. If a characteristic linear size of the confinement is large with respect to the *amplitude* order parameter correlation length then the enforced charge m decomposes into TDs bearing elementary charges m_0. These assemble at the confinement boundary and the resulting director field in the main body of the system is essentially spatially homogeneous. This behavior is consequence of mutual Coulomb-like repulsion [16] among elementary TDs. Position and number of TDs is strongly influenced by curvature of 2D surface hosting LC. Simple analysis shows that two qualitatively different elastic curvature terms exist: *intrinsic* and *extrinsic* contributions. In general both contributions are present. But in most theoretical studies so far the *extrinsic* contribution was neglected, because the derivations were based on covariant derivatives. The impact of the *intrinsic* contribution is well represented by the Effective Topological Charge Cancelation (ETCC) mechanism. It tends to *topologically neutralize* (i.e. to cancel the effective charge) each surface patch represented by an average Gaussian curvature. This is achieved either by redistribution of existing TDs or/and formation of additional pairs {*defect, antidefect*}. The ETCC mechanism in fact describes cancelation of a finite local Gaussian curvature K by dragging appropriate TDs into this region. Consequently, TDs are attracted to regions exhibiting maximal absolute value of K. On the contrary, the *extrinsic* contribution acts like a local effective ordering field the strength of which increases with curvature deviator $|C_1-C_2|/2$ [23,24,44,45], and is absent at umbilical points where $C_1=C_2$ [44]. In general, *intrinsic* and *extrinsic* contributions might have contradictory impacts on TDs. For instance, on oblate ellipsoids the *intrinsic* curvature tends to assemble TDs at the equatorial line (where K exhibits local maximum). On the contrary, for oblate shapes the*extrinsic* curvature would like to expel TDs out from the equatorial belt because the curvature deviator $|C_1-C_2|/2$ is maximal at the equatorial line. Our preliminary studies show that *extrinsic* contributions might dramatically enhance stability range of oblate-like discocytes. Such geometries are often realized in biological cells. Note that positions of TDs fingerprint relative importance of *intrinsic* and *extrinsic* curvature contributions, and can therefore serve as indicators of their relative strength. In general, deep understanding of effects of *extrinsic contributions* is important from fundamental view. Namely, it reflects impact of d-dimensional space on embedded d-1 dimensional subspace. However, lessons learned from 2D manifolds can not be directly generalized to higher dimensional systems [39]. For example, in 2D nematics only point defects exist. In 3D also line defects are possible, which can form complex knot-like structures (in bulk line defects always form closed loops). For example, topologists know how to classify all possible 2D manifolds. However, classification of all 3D manifolds remains an unsolved problem.

To illustrate possible formation of even more complex structures formed by TDs we consider glass-like states, the physics of which is still disputable. For instance, from TD perspective one could explain supercooling driven vitrification in CSBPT phases by combining well known i) Kibble mechanism [11,41], ii) Imry-Ma-Larkin (IML) mechanism [42,43], and iii) Mullins-Sekerka (MS) [46]. The universal Kibble mechanism yields conditions for which domain-type, yielding short range order, is dynamically formed.

© 2017 Global Journals Inc. (US)

Furthermore, the IML mechanism yields conditions for which domain pattern can be stabilized. It states that even infinitesimal amount of random-field type disorder stabilizes domain-type pattern. Finally, the MS mechanism provides a path via which random-field type disorder could be formed in a system. This proposed mechanism of vitrification is the topic of our current research.

References Références Referencias

1. M.C. Cross and P.C. Hohenberg, Rev. Mod. Phys. 65, 853 (1993).
2. G. Rácz, L. Dobos, R. Beck, I. Szapudi, and I. Csabai, Mon. Not. R Astron. Soc. Lett.469, L1-L5 (2017).
3. A. Hobson, American Journal of Physics 81, 211 (2013).
4. T.H.R. Skyrme, Nuclear Physics 31, 556 (1962).
5. U.K. Rößler, A.N. Bogdanov, and C. Pfleiderer, Nature442, 797 (2006).
6. T.L. Ho, Phys. Rev. Lett. 81, 742 (1998).
7. S. Meiboom, J.P. Sethna, P.W. Anderson and W.F. Brinkman, Phys. Rev. Lett. 46, 1216 (1981).
8. J.T. Giblin, J. B. Mertens, and G. D. Starkman, Phys. Rev. Lett. 116, 251301 (2016.)
9. N.D. Mermin, Rev. Mod. Phys. 51, 591 (1979).
10. P. Palffy-Muhoray, Phys. Today 60, 54 (2007).
11. T.W.B. Kibble, J. Phys. A Math.Gen. 9(8), 1387 (1976).
12. O.D. Lavrentovich, Liq. Cryst. 24, 117 (1998).
13. M.V.E. Kurik and O.D. Lavrentovich, Physics-Uspekhi 31, 196 (1988).
14. F.C. MacKintosh and T.C. Lubensky, Phys. Rev. Lett. 67, 1169 (1991).
15. M. Bowick, D.R. Nelson and A. Travesset, Phys. Rev. E 69, 041102 (2004).
16. V. Vitelli and A.M. Turner, Phys. Rev. Lett.93, 215301 (2004).
17. V. Vitelli and D.R. Nelson, Phys. Rev. E 74, 021711 (2006).
18. R.D. Kamien, Rev. Mod. Phys. 74, 953 (2002).
19. L. Mesarec, W. Góźdź, A. Iglič and S. Kralj, Scientific reports 6, 27117 (2016).
20. R.L.B. Selinger, A. Konya, A. Travesset and J.V. Selinger, J. Phys. Chem. B 115, 13989 (2011).
21. G. Napoli and L. Vergori, Phys. Rev. E 85, 061701 (2012).
22. G. Napoli and L. Vergori, Phys. Rev. Lett.108, 207803 (2012).
23. V. Kralj-Iglič, M. Remškar, G. Vidmar, M. Fošnarič, and A. Iglič, Phys. Lett. A 296, 151 (2002).
24. A. Iglč, B. Babnik, U. Gimsa, andV.Kralj -Iglič, J. Phys. A: Math. Gen. 38, 8527 (2005).
25. M. Kleman and O.D. Lavrentovich, Soft Matter Physics, Springer-Verlag, New York (2003).
26. B.S. Murray, R.A. Pelcovits, and C. Rosenblatt, Phys. Rev. E 90, 052501 (2014).
27. S. Kralj, B.S. Murray, and C. Rosenblatt, Phys Rev E. 95, 042702 (2017).
28. W. Helfrich, Zeitschriftfür Naturforschung C 28, 693 (1973)
29. S. Kralj, R. Rosso and E.G. Virga, Soft Matter 7, 670 (2011).
30. P. Kaiser, W. Wiese and S. Hess, J. Non-Equilib. Thermodyn.17, 153 (1992).
31. S. Kralj, E.G. Virga, and S. Žumer, Phys.Rev.E60, 1858 (1999).
32. H. L. Liang, S. Schymura, P. Rudquist, and J. Lagerwall, Phys. Rev. Lett. 106, 247801 (2011).
33. T. Lopez-Leon, V. Koning, K.B.S. Devaiah, V. Vitelli, and A. Fernandez-Nieves, Nature Phys. 7, 391 (2011).
34. D. Sec, T. Lopez-Leon, M. Nobili, C. Blanc, A. Fernandez-Nieves, M. Ravnik, and S. Žumer, Phys. Rev. E 86, 020705 (2012).
35. V. Vitelli and D.R. Nelson, Phys. Rev. E 74, 021711 (2006).
36. G. Skacej and C. Zannoni, Phys. Rev. Lett. 100, 197802 (2008).
37. D.S. Miller, X. Wang, and N.L. Abbott, Chem. Mater. 26, 496 (2014).
38. R.M. Wilson, Phys. Today 70 (6), 19 (2017).
39. D.R. Nelson, Nano. Lett.2, 1125 (2002).
40. W.P. Thurston and J.R. Weeks, Scient. Amer. July, 108 (1984).
41. W.H. Zurek, Nature317, 505 (1985).
42. Y. Imry and S.K. Ma, Phys. Rev. Lett. 35, 1399 (1975).
43. A.I. Larkin, Soviet Phys. JETP 31, 784 (1970).
44. V. Kralj-Iglič, B. Babnik, D. Gauger D, S. May, A. Iglič. J. Stat. Phys. 125, 727 (2006).
45. N. Walani, J. Torres and A.Agrawal. Phys. Rev. E 89, 062715 (2014).
46. J. Bechhoefer, A.J. Simon, A. Libchaber, and P. Oswald, Phys. Rev. A 40, 2042 (1989).

© 2017 Global Journals Inc. (US)

Figure caption

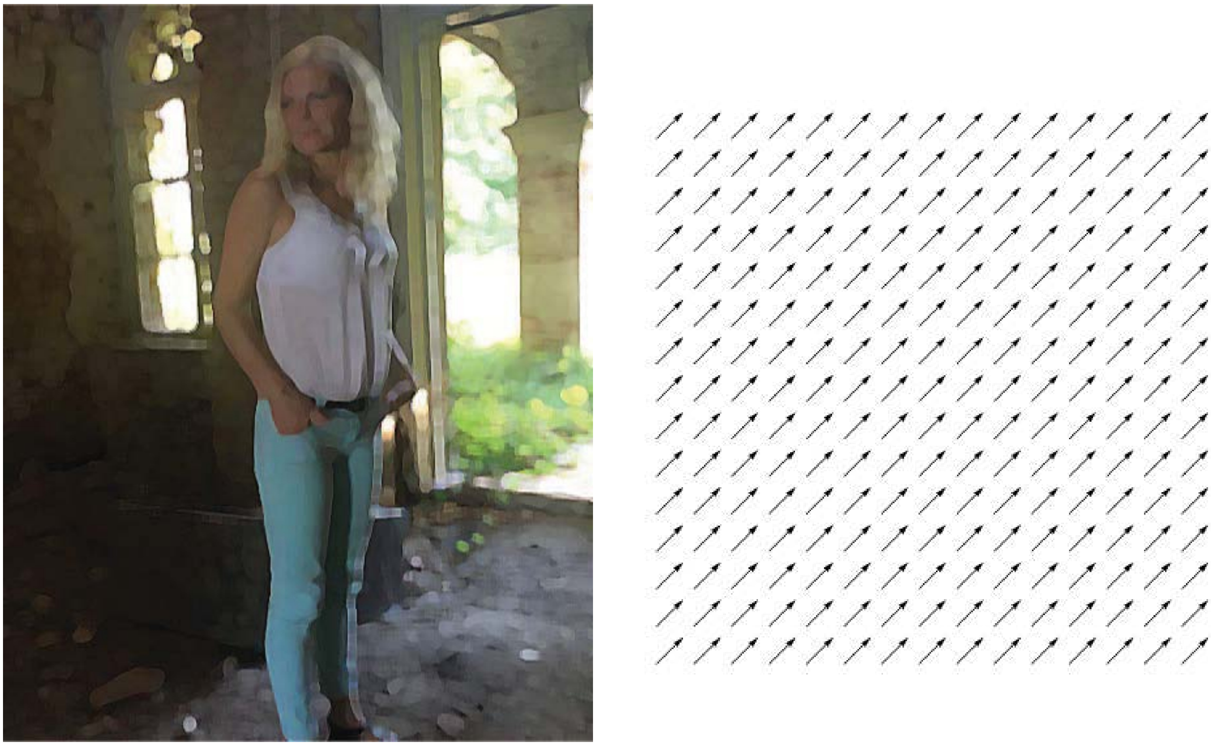

Figure 1: Could a complex pattern on left side of the figure left emerge from the field shown on the right side?

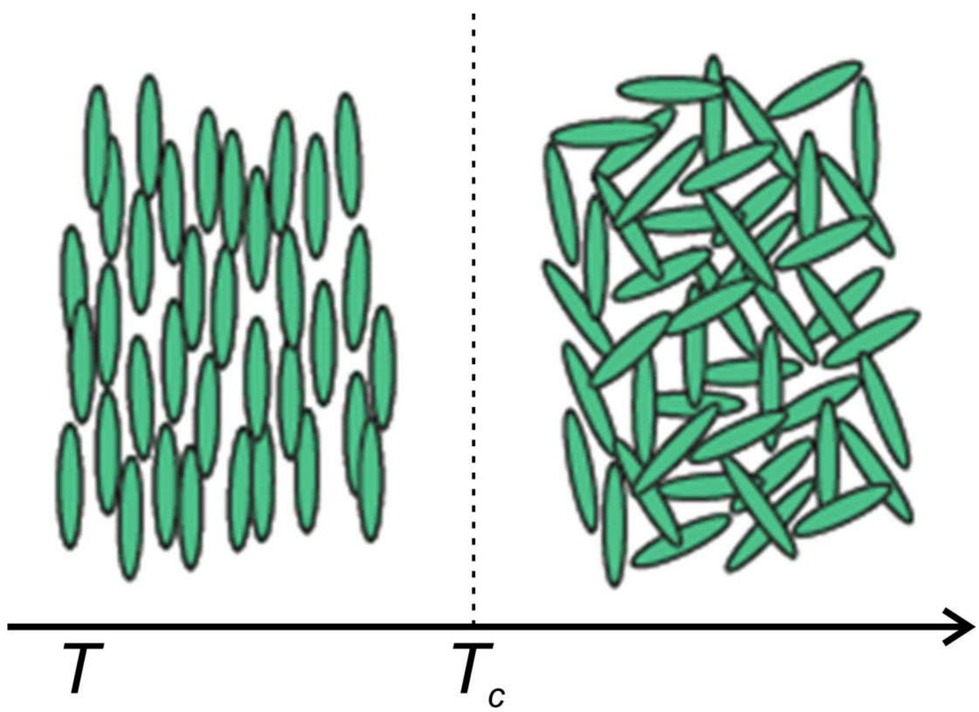

Figure 2: Temperature driven spontaneous symmetry breaking phase transition. Above T_c the system exhibits isotropic orientational symmetry where all orientations are equivalent. Below the transition the systems spontaneously aligns along a symmetry breaking direction. Any other direction would be also energetically equivalent

© 2017 Global Journals Inc. (US)

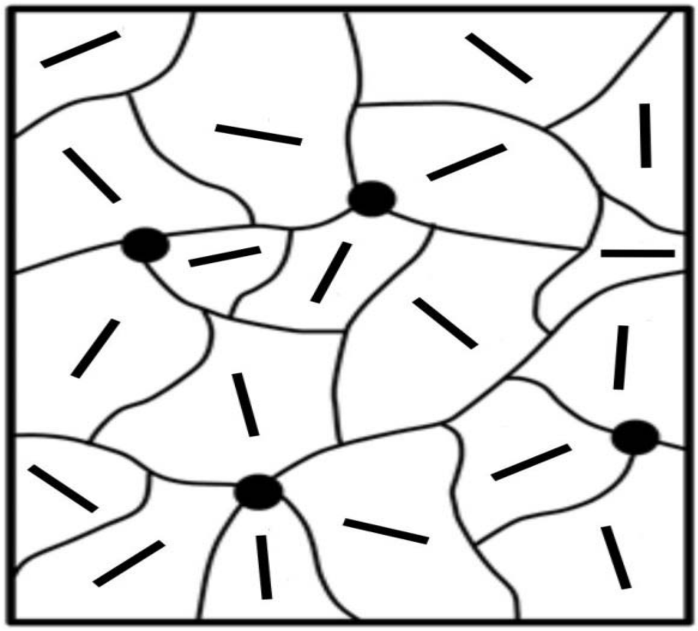

Figure 3: Domain-type pattern typically formed in a fast enough continuous symmetry breaking phase transition. In general in different parts of the system a different symmetry breaking direction because these parts are informationally decoupled. Lines indicate domain walls. Average orientational ordering within each domain is depicted with a thick line. Circles indicate presence of topological defect which are locally stable for fixed boundary conditions. In general average domain size grows in time which is enabled by annihilation of pairs {*defect, antidefect*}

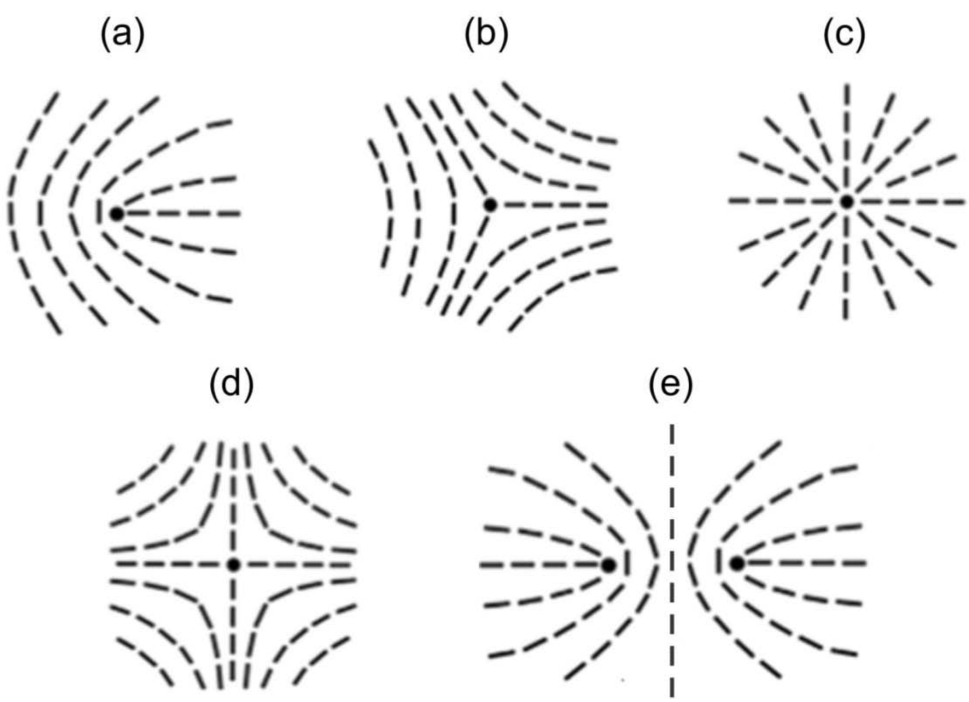

Figure 4: Typical topological defects in two-dimensions characterized by the winding number m. (a) m=1/2, (b) m=-1/2, (c) m=1, (d) m=-1. In (e) am=1 TD is split into two m=1/2 TDs. Winding numbers with minimal value $|m|=1/2$ are referred to as *elementary* topological charges $\theta_0 = 0$.

© 2017 Global Journals Inc. (US)

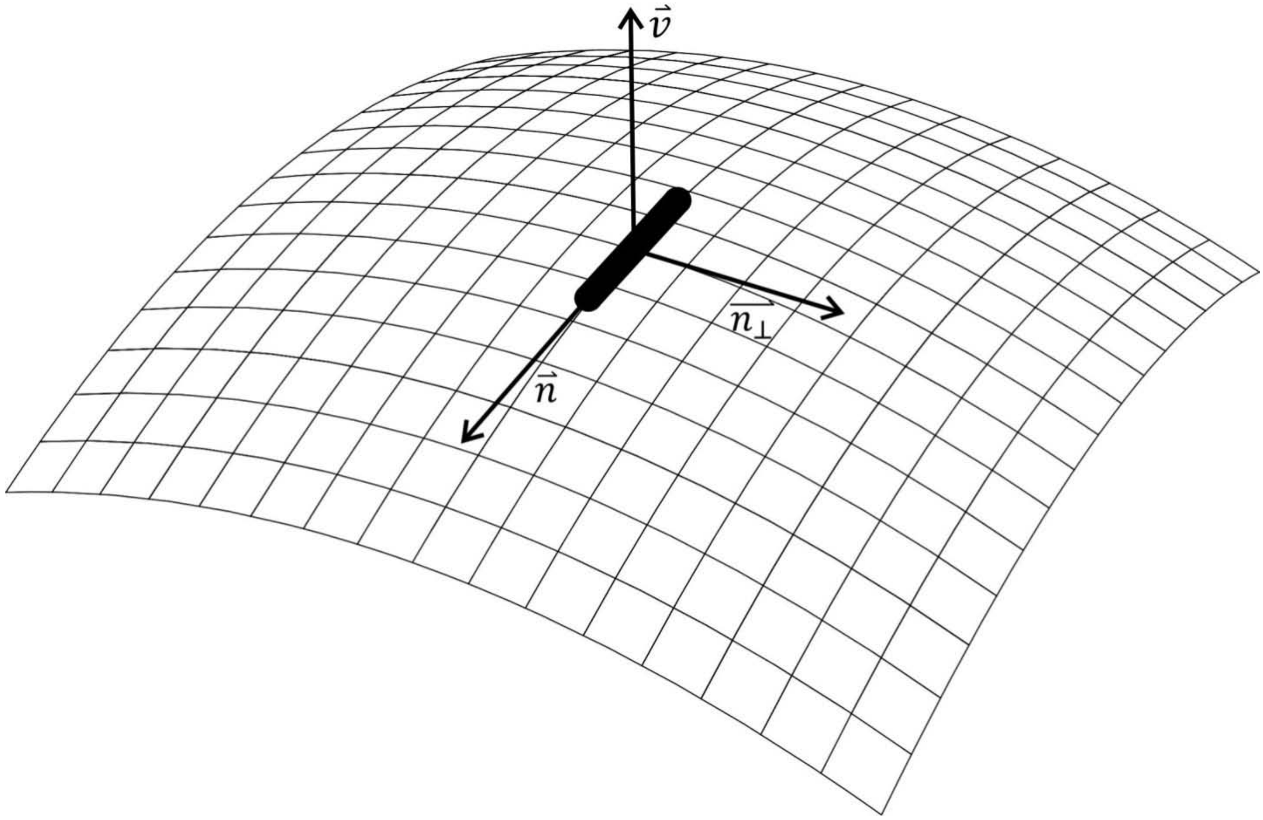

Figure 5: Orientational ordering with a 2D curved surface is at mesoscopic scale described by the uniaxial nematic director field $\vec{n}$. Local surface orientation is defined by the unit normal $\vec{v}$

© 2017 Global Journals Inc. (US)

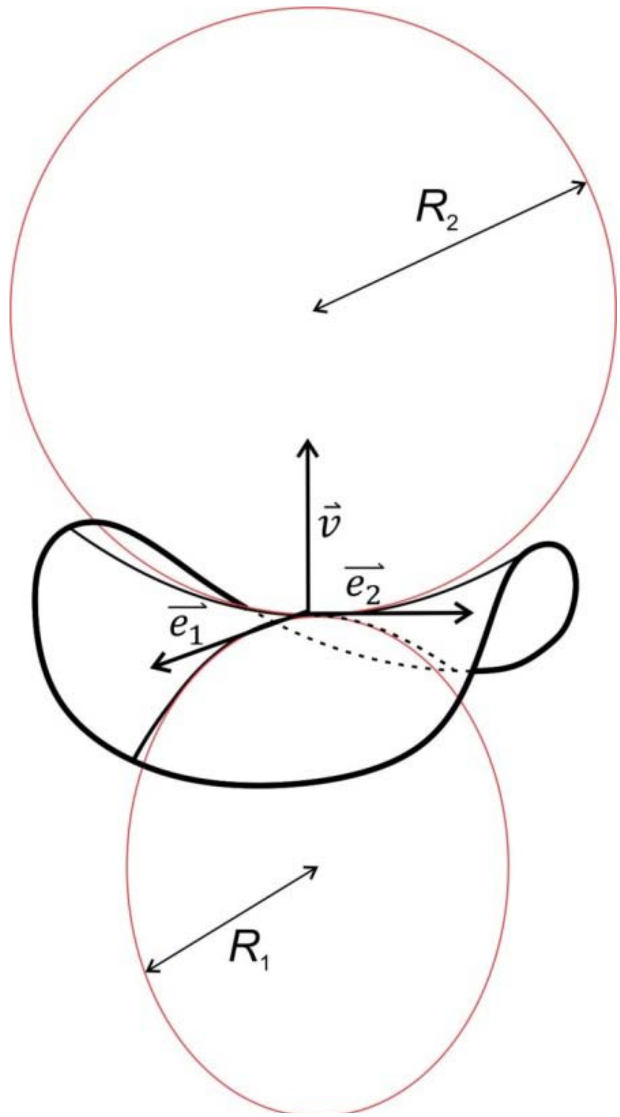

Figure 6: Sketch of a principal curvature frame $\{\vec{e}_1, \vec{e}_2\}$ and the corresponding curvature radios$\{R_1$, $R_2\}$. The corresponding principal curvatures are given by$\{C_1 = 1/R_1, C_2 = 1/R_2\}$

© 2017 Global Journals Inc. (US)

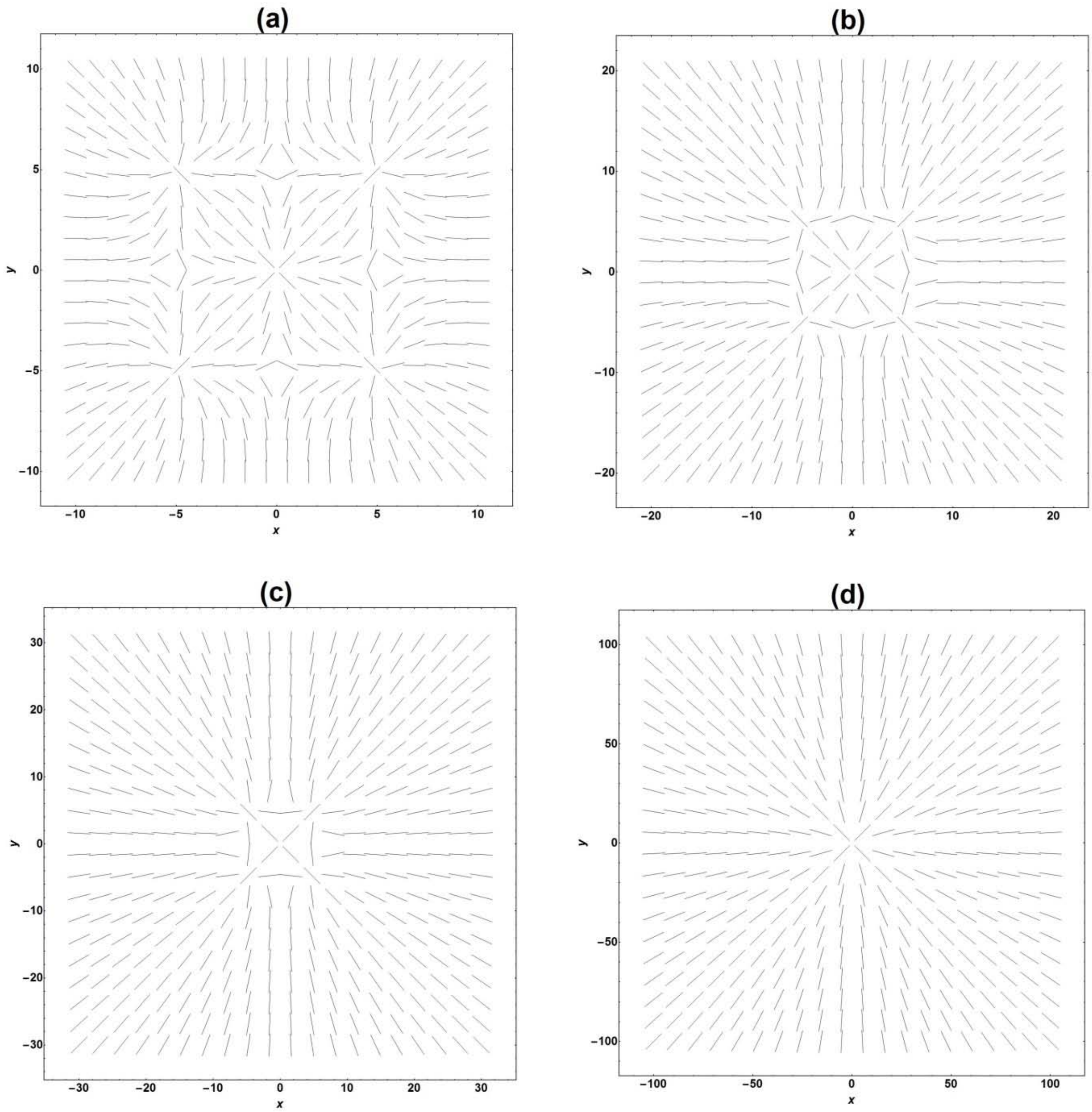

Figure 7: A checkerboard lattice of nine TDs bearing topological charges $m = \pm 1$. The central TDs bears charge $m = 1$. The coordinate system is presented in distance unitsa_0. In each line neighboring TDs are separated for a distance 5 a_0. In figures (a), (b), (c), (d) we progressively zoom out the viewing are of lattice of TDs. In (a) the resolution is high enough to see all nine TDs. In (b) we see only the effective far-distance field of the lattice, which bears the total topological charge $m = 1$

© 2017 Global Journals Inc. (US)

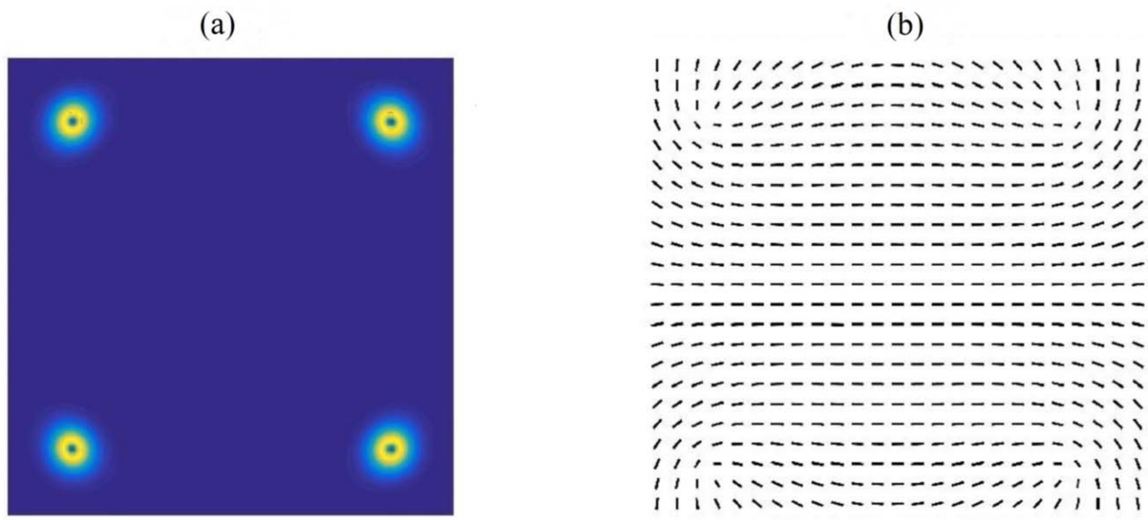

Figure 8: The square boundary enforces the total topological charge $m=2$ to the system. The characteristic linear size R of the system is large with respect to the order parameter correlation length ξ. The enforced charge $m=2$ splits into four m=1/2 *elementary* charges which assemble in the corners of the square in order to maximize their mutual separation. $R/\xi=10$. (a) 2D biaxiality profile β^2 in which cores of TDs are clearly visible. (b) The corresponding director field profile. Note that the director field is essentially homogeneous in the central part of the structure

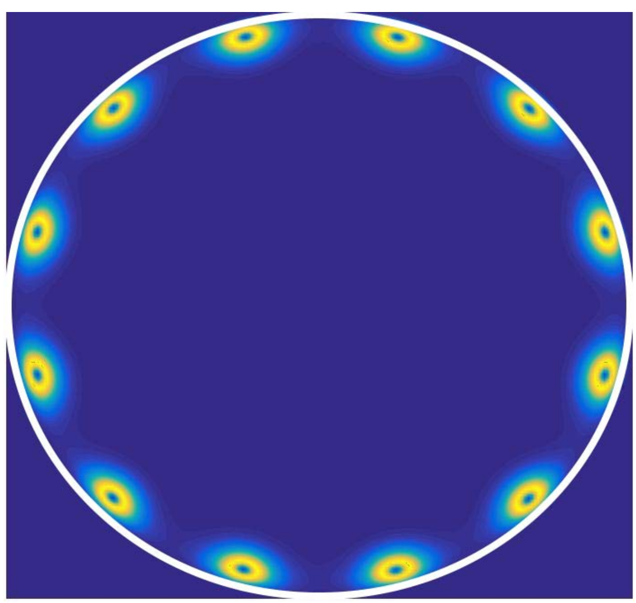

Figure 9: Within the circle we enforce the total topological charge $m=6$, which splits into 12 $m=1/2$ *elementary* charges. These are well visible in the 2D biaxiality β^2 plot. The director field in the central part of the figure is essentially spatially homogeneous aligned along a single symmetry breaking direction. $R/\xi=10$

© 2017 Global Journals Inc. (US)

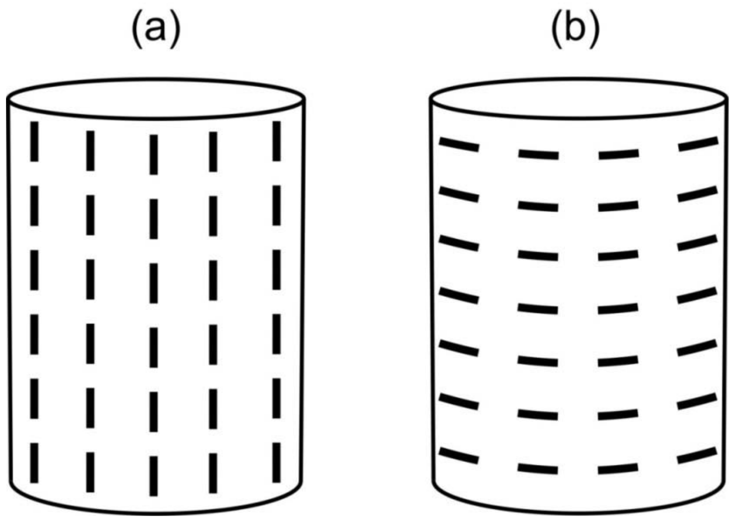

Figure 10: In both structures (a) and (b) the *intrinsic* contribution equals zero. On the contrary, the *extrinsic* contribution is lower in (a)

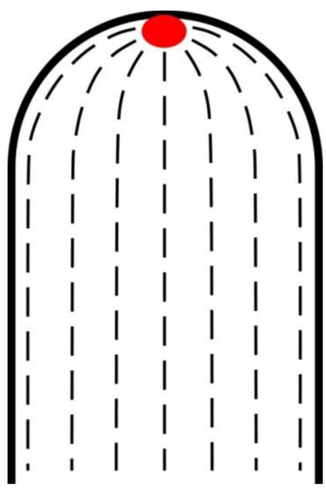

Figure 11: Schematic sketch illustrating tendency of TDs (red point) with $m=1$ to be localized in the region with $K>0$. In this case the elastic penalty of the director structure in the cylindrical part of the system equals zero because the structure is there spatially homogeneous

Global Journal of Science Frontier Research (A) Volume XVII Issue III Version I Year 2017

© 2017 Global Journals Inc. (US)

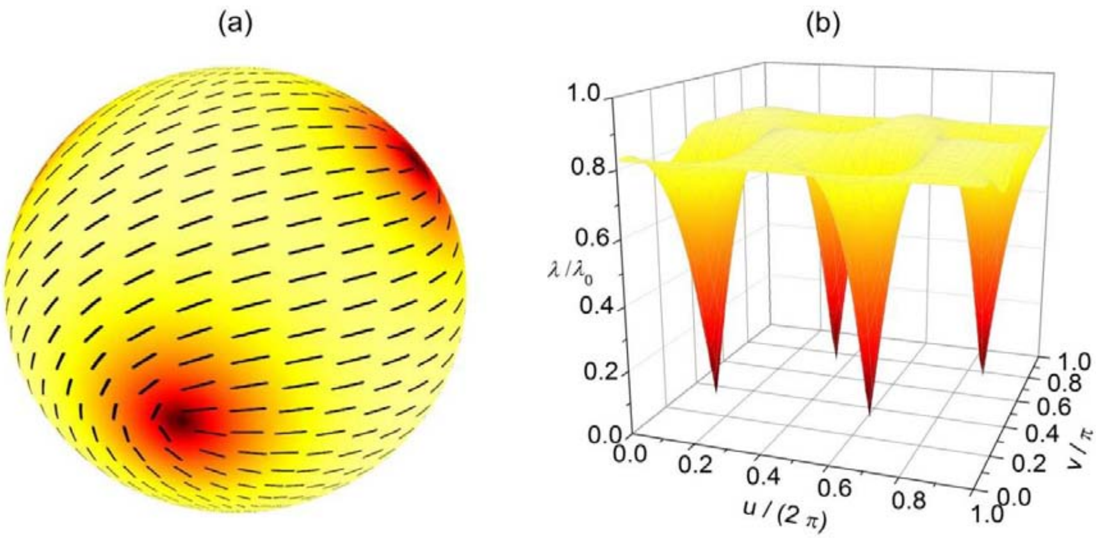

Figure 12: A sphere hosting four $m=1/2$ TDs. (a) The nematic director field and *amplitude* profile superimposed on the sphere. (b) Order parameter *amplitude* in the (u,v) plane. The TDs reside at the vertices of hypothetically inscribed tetrahedron in order to maximize their mutual separation. $R/\xi=5$

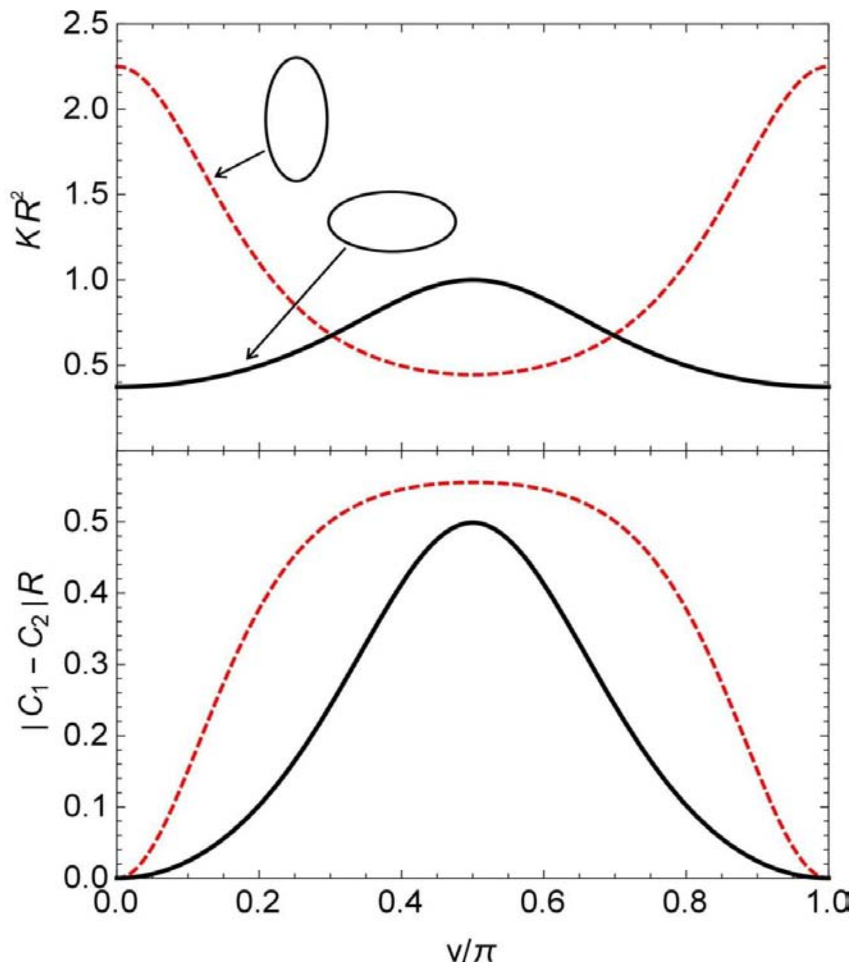

Figure 13: Gaussian curvature (upper panel) and absolute difference between principal curvatures (bottom panel) in prolate (dashed curve) and oblate (full line) ellipsoids. R denotes minimal radius describing an ellipsoid. Red dashed lines represent the prolate ellipsoid $a/b=1.5$, while the black lines represent the oblate ellipsoid $b/a=1.28$, see Eq.(10b)

© 2017 Global Journals Inc. (US)

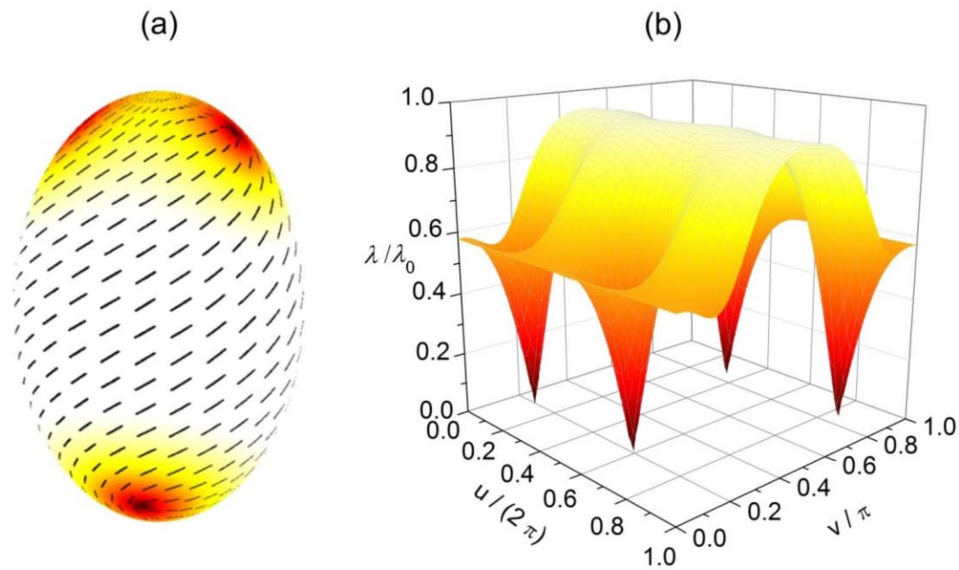

Figure 14: (a) An ellipsoidal shell with superimposed nematic director and amplitude profile. The ''real'' TDs are assembled at the poles, where the negative smeared Gaussian charge builds up due to the localized positive Gaussian curvature. (b) The order parameter profile in the (u,v) plane revealing exact positions of $m=1/2$ TDs. $R/\xi = 5$, $k_e=0$

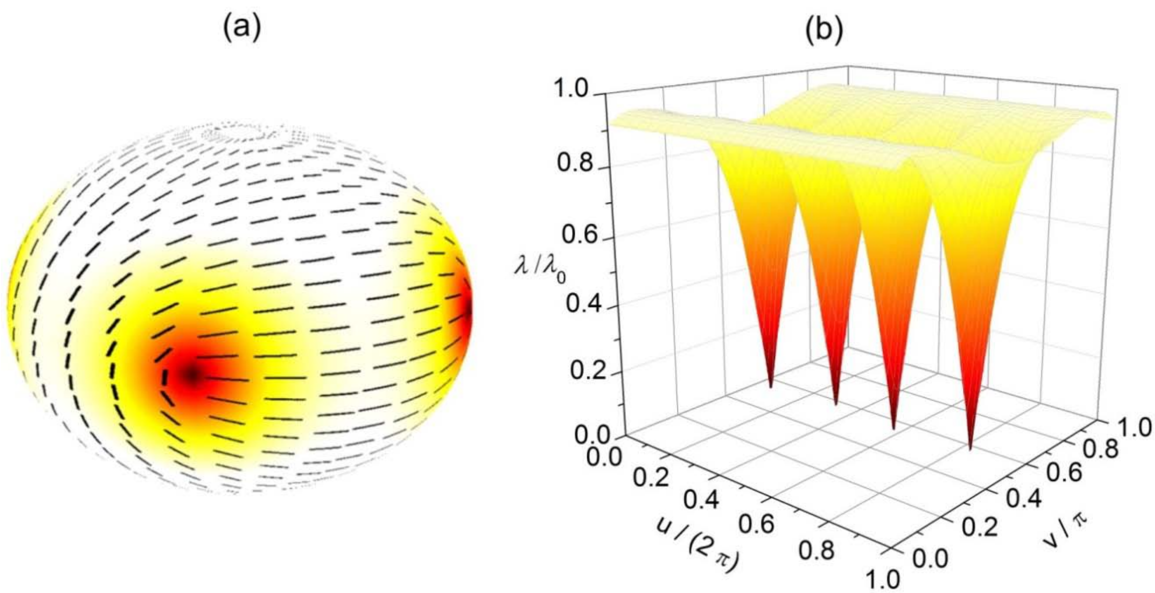

Figure 15: (a) Nematic director and order parameter *amplitude* superimposed on the oblate shell. (b) The *amplitude* plotted in the (u,v) plane. $R/\xi = 5$, $k_e=0$

© 2017 Global Journals Inc. (US)

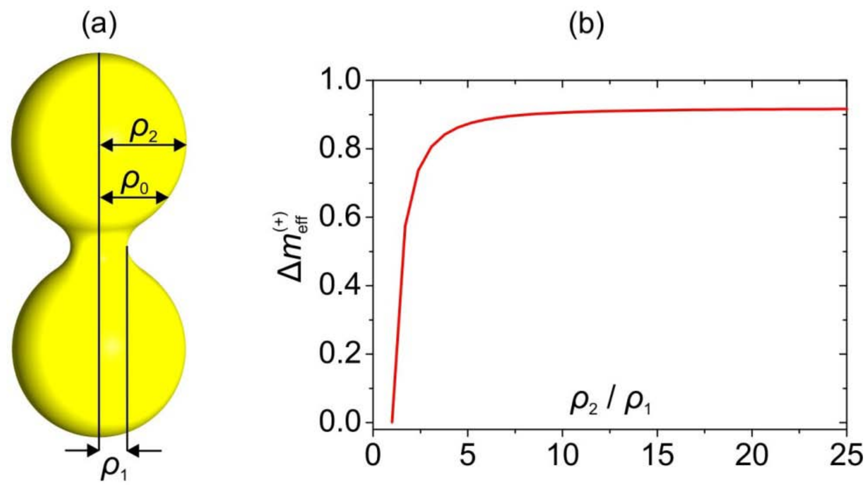

Figure 16: (a) An axially symmetric dumb-bell structure. It is characterized by distances ρ_2 (maximal radius), ρ_1 (minimal radius). The radius ρ_0 separates regions with positive ($\rho > \rho_0$) and negative ($\rho_0 > \rho$) Gaussian curvature. (b) Building up of effective topological charge in regions with positive Gaussian curvature ($\rho > \rho_0$)

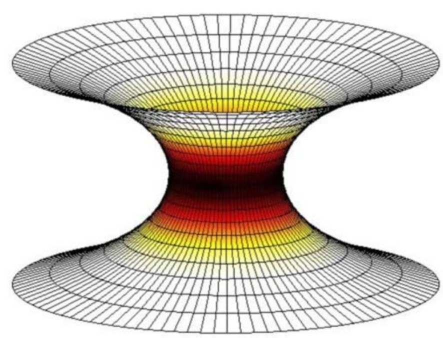

Figure 17: Catenoid With The Superimposed *Amplitude* Field. The Meaning Of The Color Code Is Visible From Figure 18a

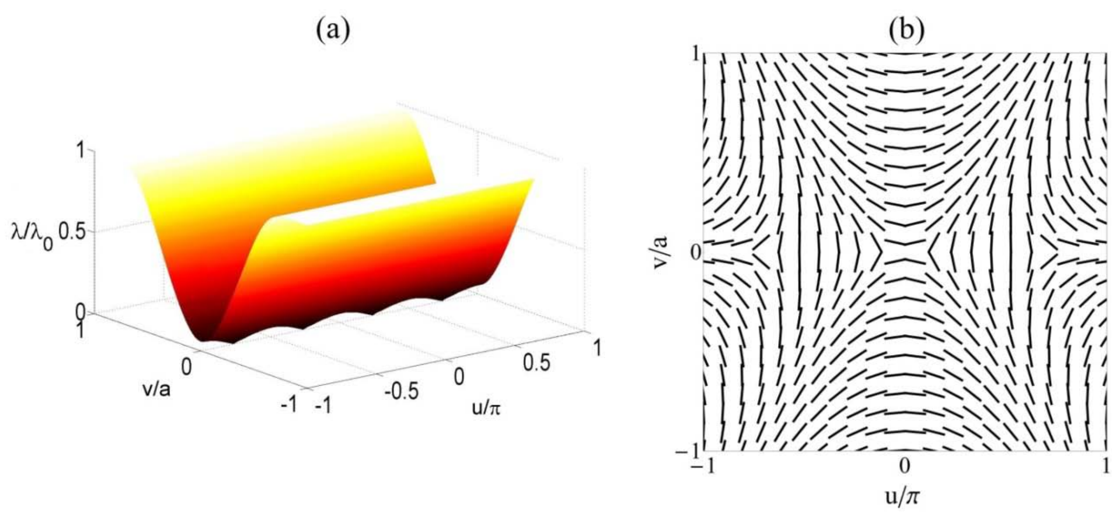

Figure 18: (a) Four m=-1/2 TDs residing at the neck of the catenoid shown in Figure 17. (b) The corresponding nematic director field. $R/\xi = 0.1$, R is the catenoid's neck radius

© 2017 Global Journals Inc. (US)

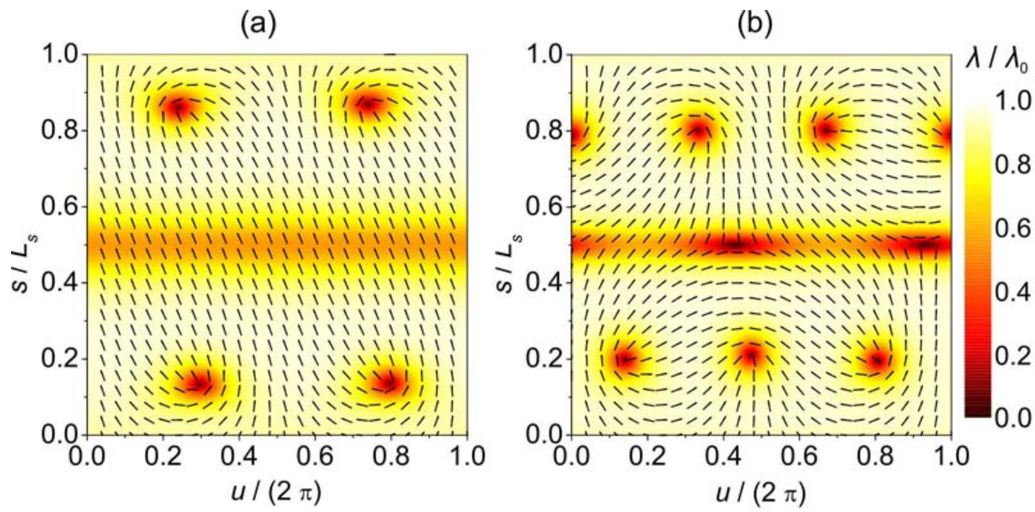

Figure 19: Configuration of TDs in the dumb-bell structure shown in Figure 16 just below (a) and above (b) the critical condition where two pairs {*defect,antidefect*} are formed. $R/\xi = 5$, $k_e = 0$

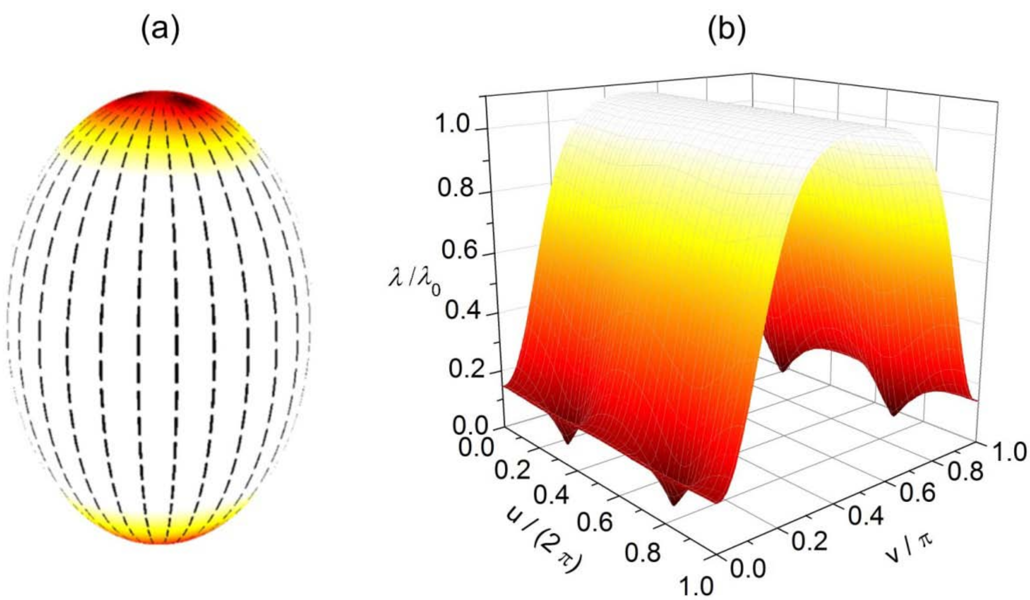

Figure 20: (a) A prolate ellipsoid with superimposed order parameter field for a relatively strong *extrinsic* curvature. (b) *Amplitude* field in the (u,v) plane. $R/\xi = 5$, $k_e/k_i = 1$

© 2017 Global Journals Inc. (US)

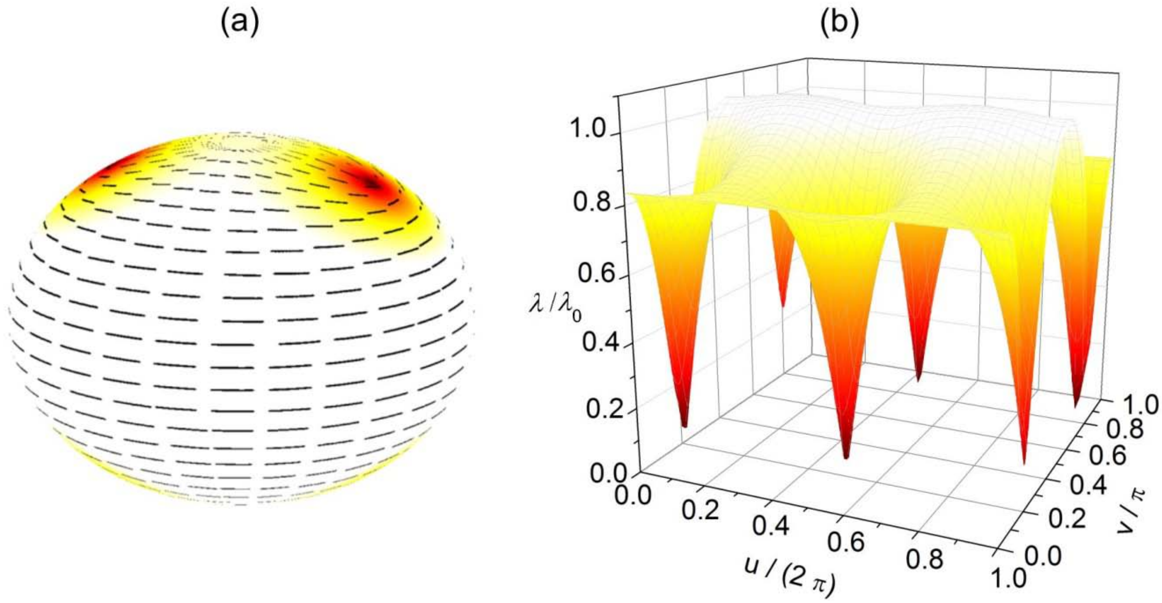

Figure 21: (a) An oblate ellipsoid with superimposed order parameter field for a relatively strong *extrinsic* curvature. (b) *Amplitude* field in the (u,v) plane. $R/\xi = 5$, $k_e / k_i = 1$

© 2017 Global Journals Inc. (US)